AIAA SciTech Forum
5-9 January 2015, Kissimmee, Florida
53rd AIAA Aerospace Sciences Meeting

10.2514/6.2015-1673

Simplified Aerodynamics Models to Predict the Effects of Upstream Propellers on Wing Lift

Michael D. Patterson* and Brian J. German†
Georgia Institute of Technology, Atlanta, GA, 30332, U.S.A.

In this paper we describe simple, two-dimensional aerodynamic models that incorporate the effects of the propeller installation angle to quickly estimate the lift augmentation from configurations in which multiple propellers are distributed upstream of a wing. The approach predicts variations in the apparent lift curve slope and zero-lift angle of attack of airfoils in the presence of propeller slipstreams of varying height. The angle of the slipstream relative to the airfoil and the height of the slipstream are both shown to have significant impacts on the lift augmentation. The methods presented in this paper are intentionally simple and can be used to help build a designer's intuition about the effects of distributed leading edge propellers employed as high-lift devices.

Nomenclature

a_0	Lift curve slope	α	Angle of attack
b	Span	β	Slipstream height ratio
c	Chord length	Γ	Circulation
C_L	Lift coefficient	κ	Circulation multiplier
c_l	Section lift coefficient	ρ	Density
h	Semiheight of propeller slipstream	φ	Propeller installation angle
i_p	Propeller slipstream inclination angle	Subscripts	
K_{a_0}	Lift curve slope multiplier	ep	Effective value aft of the propeller
K_L	Lift multiplier	g	Geometric
L	Lift	j	Jet
q	Dynamic pressure	$L=0$	Zero-lift
V	Velocity	p	Propeller
w	Induced velocity	∞	Freestream

I. Introduction

Recently, NASA has been studying the potential impacts of electric propulsion technologies on the design of aircraft.[1–4] Because electric motors are much smaller and lighter than conventional engines, these motors can be placed in many different locations on the aircraft more easily than conventional engines. Additionally, because electric motors are a near "scale-free" technology,[1] it is possible to distribute many smaller electric motors without encountering large efficiency reductions or weight penalties. These properties of electric motors enable designers to distribute motors and propellers to achieve synergistic aeropropulsive coupling, as well as structural, control, and safety benefits.

One configuration that employs such aeropropulsive coupling incorporates multiple propellers distributed upstream of the wing leading edge along the entire span as shown in Figure 1(a). These leading edge propellers are operated only at low-speed flight conditions to increase the speed of the airflow over the wing in order to increase the lift; therefore, they are more appropriately viewed as a form of high lift device

*Ph.D. Candidate, School of Aerospace Engineering, 270 Ferst Drive. Student Member AIAA.
†Associate Professor, School of Aerospace Engineering, 270 Ferst Drive. Senior Member AIAA.

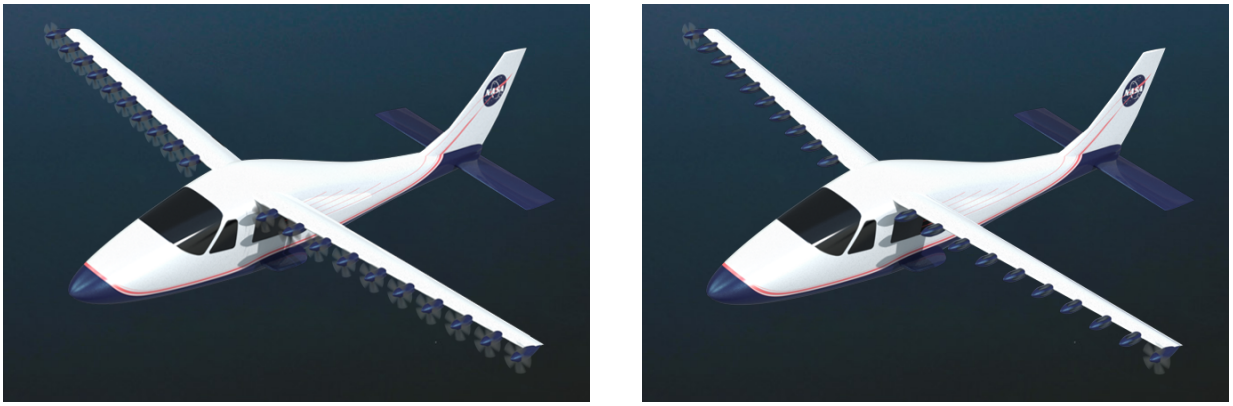

(a) Low-speed propeller configuration

(b) Higher-speed propeller configuration

Figure 1. NASA Leading Edge Asynchronous Propellers Technology (LEAPTech) distributed electric propulsion concept proposed by Moore and Fredericks[1]

rather than a propulsive device. For higher-speed conditions, the leading edge propellers are folded as shown Figure 1(b), and all thrust is generated by the tip propellers. Such a configuration is potentially advantageous because the wing size can be reduced while maintaining adequate low-speed performance, which increases the cruise efficiency of the aircraft.[2]

In this paper we will describe two simple aerodynamic models that can be used in the early conceptual design stage to aid designers of aircraft similar to that shown in Figure 1. These models provide insights into the physics and fundamental tradeoffs inherent in these designs. We begin by defining the geometry that will be considered throughout the paper. Next, we develop aerodynamic models under the assumption that the propeller slipstream height is very large. Finally, we modify the approach to account for cases in which the slipstream height is finite.

II. Geometry

In this paper we consider configurations in which propellers are installed upstream of a wing, and the two-dimensional geometry under consideration is shown in Figure 2. The figure shows the orientation of the freestream velocity vector ($\boldsymbol{V_\infty}$), the propeller disk plane, the slipstream velocity from the propeller ($\boldsymbol{V_p}$), and the local wing section chord line relative to the reference chord line of the wing. The airfoil at any given wing section may be twisted from the wing reference chord by an angle α_{twist}, and positive twist is shown in the figure. The propeller is located forward of the wing and is inclined at an angle of φ relative to the wing frame's vertical; a positive φ is shown in the figure and indicates an upward tilt of the resultant thrust vector from the propeller relative to the wing reference chord.

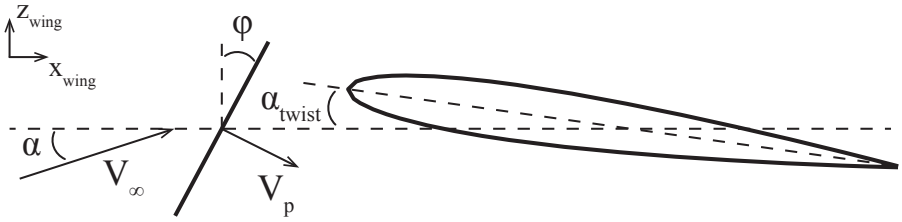

Figure 2. A two-dimensional cross section of the geometry under consideration relative to the wing reference frame.

The geometry in Figure 2 can be formulated instead relative to the local airfoil's chord line as shown in Figure 3. In the local reference frame of the airfoil sections, only two angles, α_g and i_p, describe the direction of the incoming velocity vectors $\boldsymbol{V_\infty}$ and $\boldsymbol{V_p}$, respectively. The local geometric angle of attack, α_g, can be

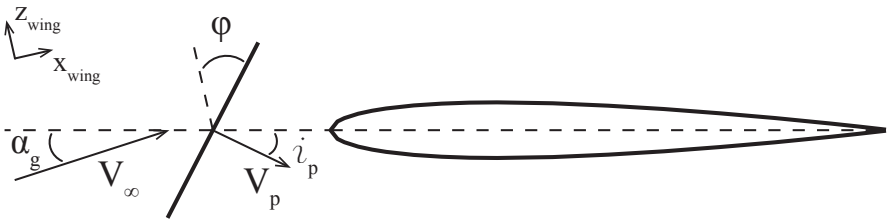

Figure 3. Orientation of freestream velocity and propeller disk with respect to a local airfoil section

written in terms of the local twist and the wing angle of attack as Eq. 1.

$$\alpha_g = \alpha + \alpha_{\text{twist}} \tag{1}$$

Consistent with momentum theory,[5–7] we model the propeller slipstream as a uniform velocity oriented in the direction of the disk normal axis. With the assumption that $\boldsymbol{V_p}$ is perpendicular to the propeller disk, the incoming angle of the slipstream, i_p, can be written in terms of the local twist and the propeller installation angle as Eq. 2.

$$i_p = \varphi - \alpha_{\text{twist}} \tag{2}$$

Because we will focus on two-dimensional geometry throughout the paper, we will refer to the geometry in terms of the local variables i_p and α_g as opposed to the variables φ and α.

The slipstream from the propeller causes a change in the effective angle of attack of the airfoil as illustrated in Figure 4. The effective angle of attack behind the propeller, α_{ep}, is defined between the chord line and the effective velocity behind the prop, V_{ep}, which is a vector sum of the freestream and slipstream velocities (i.e., $\boldsymbol{V_{ep}} = \boldsymbol{V_\infty} + \boldsymbol{V_p}$).

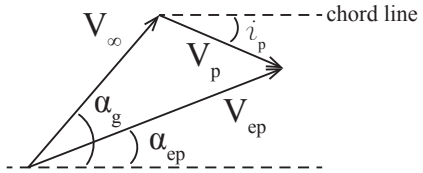

Figure 4. Vector diagram showing the effective angle of attack behind the prop resulting from the axial component of the propwash over the wing

An expression for the effective angle of attack of the airfoil section behind the propeller in terms of the geometric angle of attack, the freestream velocity, the velocity of the slipstream, and the local slipstream inclination angle is given in Eq. 3. This relationship is derived from the geometry presented in Figure 4.

$$\tan(\alpha_{ep}) = \frac{V_\infty \sin(\alpha_g) - V_p \sin(i_p)}{V_\infty \cos(\alpha_g) + V_p \cos(i_p)} \tag{3}$$

For small angles of attack and small inclination angles, Eq. 3 can be reduced to Eq. 4.

$$\alpha_{ep} \approx \frac{V_\infty \alpha_g - V_p i_p}{V_\infty + V_p} = \frac{\alpha_g - (V_p/V_\infty)\, i_p}{1 + (V_p/V_\infty)} \tag{4}$$

Finally, the magnitude of the effective local velocity behind the propeller can also be determined from the geometry in Figure 4 as Eq. 5.

$$V_{ep} = \sqrt{V_\infty^2 + 2V_\infty V_p \cos(\alpha_g + i_p) + V_p^2} \tag{5}$$

III. A Two-Dimensional Model for Predicting Wing Lift Augmentation from Leading Edge Propellers

In this section we develop a simple model that captures some of the main effects of the propeller slipstream on wing lift. The model is intended to provide design insights and enable "back of the envelope" calculations that may provide a starting point for more detailed studies with higher-order models. The model involves many simplifying assumptions and consequently should be used with caution and only in conjunction with more detailed analyses.

The simplest estimation of the wing lift increase in the presence of a propeller slipstream can be made by assuming that the lift is proportional to the dynamic pressure. In this case the percentage increase in the lift per unit span of an airfoil section is simply the percentage increase in the dynamic pressure as shown in Eq. 6.

$$\frac{\Delta L'}{L'_\infty} = \frac{\Delta q}{q_\infty} \tag{6}$$

However, this estimation ignores any effects of the propeller installation angle, which essentially assumes that the angle of attack of the airfoil remains unchanged when immersed in the propeller slipstream. As is clear from inspection of Figure 4, this is a poor assumption, and this model is insufficient to describe the lift augmentation from upstream propellers.

We will assume that the geometry of any local airfoil section with an upstream propeller can be represented as shown in Figure 5. The propeller diameter is viewed to be large in comparison to the wing chord and the propeller is installed in front of the wing with little offset above or below the chord line such that the wing section will be completely immersed in the slipstream from the propeller. We represent the airfoil by a single

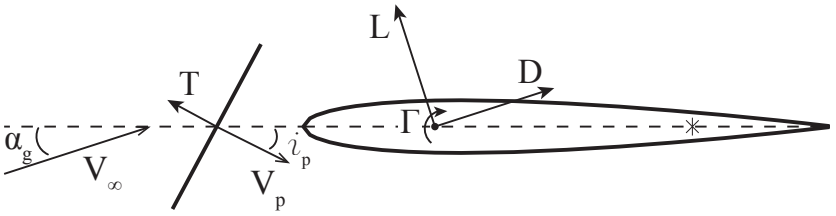

Figure 5. The geometry describing a two dimensional point vortex representation of an airfoil and the incoming local frestream velocity and propeller slipstream velocity relative to the local airfoil section

point vortex of circulation strength Γ, which is placed at the quarter chord point. The circulation strength is determined by requiring flow tangency at a control point located at the 3/4 chord point, which is denoted by an asterisk (*) in Figure 5. We will assume that the airfoil is symmetric or is sufficiently thin such that the control point and point vortex are located on the chord line of the airfoil, which implies that the point vortex will induce a velocity, w, downward and normal to the chord line at the control point. For a known required induced velocity at the control point, the circulation strength of a point vortex can be found from Eq. 7,[8] where c is the chord length of the airfoil.

$$\Gamma = \pi c w \tag{7}$$

Once the circulation strength is known, the lift force per unit span from the vortex can be determined from the scalar form of the Kutta-Joukowski theorem presented in Eq. 8, where the lift per unit span acts perpendicular to the incoming velocity in the plane of the airfoil.

$$L' = \rho V \Gamma \tag{8}$$

Figure 6 shows the required induced velocity from the point vortex, w_∞, if only the freestream velocity is present. The larger the vertical component of the freestream velocity ($V_\infty \sin(\alpha_g)$), the larger the magnitude of the circulation will be required to enforce flow tangency. Because the local lift per unit span is directly proportional to the circulation strength, this method predicts that increases in α_g will produce increases in lift proportional to the magnitude of the increase of α_g.

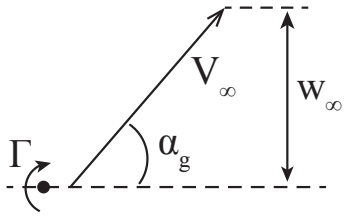

Figure 6. Vector diagram showing the geometric angle of attack and required induced velocity from a point vortex to create flow tangency in the presence of the freestream velocity

If a propeller is installed upstream of the airfoil, an additional velocity component is added to the freestream as was illustrated in Figure 4. However, in addition to the changing orientation and magnitude of the total velocity vector, we are also concerned with the strength of the point vortex, Γ. As with the isolated airfoil, the vortex strength is determined by maintaining flow tangency at the control point. Here, the magnitude of Γ will vary based on the magnitude of the vertical component of the effective velocity aft of the propeller, $V_{ep}\sin(\alpha_{ep})$. To determine the change in the magnitude of the circulation compared to the baseline, we are interested in the change between the induced velocity required with only the freestream, w_∞, and the new induced velocity required in the presence of the new total velocity, w_{new}. If $w_{\text{new}} < w_\infty$, then the new circulation strength will be decreased; if $w_{\text{new}} > w_\infty$, then the new circulation strength will be increased.

A. Specific Propeller Installations

In this subsection we consider four propeller installations whose velocity vector diagrams are shown in Figure 7. For each case, the original lift per unit span resulting from only the freestream velocity is denoted as $L'_\infty = \rho V_\infty \Gamma_\infty$, where Γ_∞ is the circulation strength determined from the induced velocity w_∞ (as illustrated in Figure 6). The new lift per unit span in the presence of the propeller slipstream will be $L'_{\text{new}} = \rho V_{ep}\Gamma_{\text{new}}$, where Γ_{new} is the circulation strength determined from the induced velocity w_{new}. The change in the lift between these two conditions is $\Delta L' = L'_{\text{new}} - L'_\infty$.

In the following subsections, the implications of the four propeller installations on the lift per unit span are discussed. The direct contribution of the thrust vector to lift will be ignored for simplicity in the following analyses unless otherwise noted.

1. Propeller Inclined Upward

For the case shown in Figure 7(a) in which $i_p > 0$, we expect the circulation to decrease relative to the unblown wing because $w_{\text{new}} < w_\infty$. Additionally, the angle of attack of the airfoil is decreased ($\alpha_{ep} < \alpha_g$), which has two potentially detrimental consequences:

1. The local lift per unit span vector is tilted aft in the drag direction by the angle $\alpha_g - \alpha_{ep}$, which implies that not all the force produced by the airfoil is usable for lift, and some directly contributes to drag.

2. In case of propeller loss, the airfoil angle of attack will suddenly increase, potentially causing stall.

If the circulation strength decreases by some factor κ (where $\kappa < 1$), then $\Gamma_{\text{new}} = \kappa\Gamma_\infty$ and the percentage increase in the lift can be expressed as Eq. 9.

$$\frac{\Delta L'}{L'_\infty} = \kappa\frac{V_{ep}}{V_\infty} - 1 \tag{9}$$

Note that if $\kappa = 1$, Eq. 9 reduces to $\Delta L'/L'_\infty = \Delta V/V_\infty$; therefore, this installation should result in an increase in lift per unit span *less* than the increase in the total velocity because $\kappa < 1$.

Because the induced velocity from a point vortex is directly proportional to the vortex strength, κ can be expressed in terms of induced velocity ratio as shown in Eq. 10.

$$\kappa = \frac{w_{\text{new}}}{w_\infty} = 1 - \frac{V_p \sin i_p}{V_\infty \sin\alpha_g} \tag{10}$$

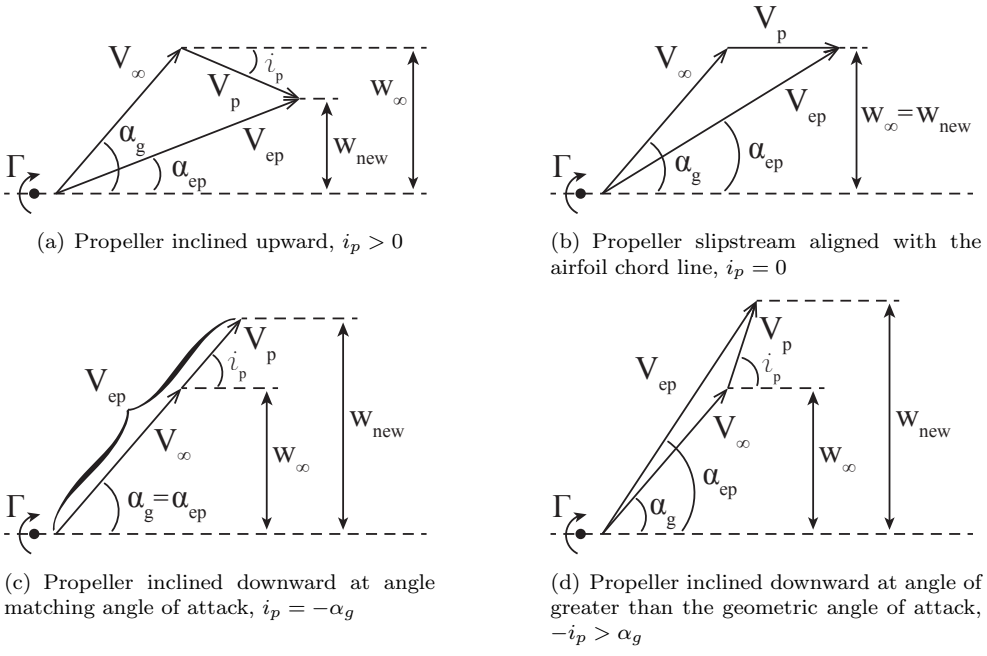

(a) Propeller inclined upward, $i_p > 0$

(b) Propeller slipstream aligned with the airfoil chord line, $i_p = 0$

(c) Propeller inclined downward at angle matching angle of attack, $i_p = -\alpha_g$

(d) Propeller inclined downward at angle of greater than the geometric angle of attack, $-i_p > \alpha_g$

Figure 7. Vector diagrams showing the effective angle of attack and required induced velocity from a point vortex for various propeller installation angles

The percentage change in the lift can then be expressed in terms of the freestream velocity, local slipstream velocity, local propeller inclination angle, and geometric angle of attack as Eq. 11.

$$\frac{\Delta L'}{L'_\infty} = \left(1 - \frac{V_p \sin i_p}{V_\infty \sin \alpha_g}\right) \frac{\sqrt{V_\infty^2 + 2V_\infty V_p \cos(\alpha_g + i_p) + V_p^2}}{V_\infty} - 1 \tag{11}$$

Finally, the percentage increase in lift per unit span can be represented in terms of the dynamic pressure as shown in Eq. 12.

$$\frac{\Delta L'}{L'_\infty} = \frac{q_{\text{new}} (\sin \alpha_{ep} / \sin \alpha_g) - q_\infty}{q_\infty} \tag{12}$$

Here, $\sin \alpha_{ep} / \sin \alpha_g < 1$ because $\alpha_{ep} < \alpha_g$; therefore, Eq. 12 indicates that the lift increase will be less than the percentage change in the dynamic pressure.

2. Propeller Normal Axis Aligned with the Local Airfoil Chord

The case shown in Figure 7(b) in which the propeller's slipstream is aligned with the airfoil chord line is identical to that presented above in Section III.A.1 except that the circulation strength is unchanged from the unblown wing (i.e., $\Gamma_{\text{new}} = \Gamma_\infty$). With this constant circulation strength, the percentage increase in lift is equivalent to $\Delta V / V_\infty$, as shown in Eq. 13.

$$\frac{\Delta L'}{L'_\infty} = \frac{\rho V_{ep} \Gamma_\infty - \rho V_\infty \Gamma_\infty}{\rho V_\infty \Gamma_\infty} = \frac{V_{ep}}{V_\infty} - 1 = \frac{\Delta V}{V_\infty} \tag{13}$$

Additionally, the angle of the incoming propeller slipstream is zero, so the percentage increase in lift can also be expressed as Eq. 14.

$$\frac{\Delta L'}{L'_\infty} = \frac{\Delta V}{V_\infty} = \frac{\sqrt{V_\infty^2 + 2V_\infty V_p \cos \alpha_g + V_p^2}}{V_\infty} - 1 \tag{14}$$

3. Propeller Normal Axis Aligned with the Freestream Velocity

For the case shown in Figure 7(c) in which the propeller slipstream is aligned with the freestream velocity (i.e., $i_p = -\alpha_g$) we expect the circulation strength to increase compared to the unblown case because $w_{\text{new}} > w_\infty$, which will increase the lift produced. Also, the effective angle of attack of the airfoil is the same as the geometric angle of attack (i.e., $\alpha_{ep} = \alpha_g$), which implies that there is no tilting of the lift vector and that if a propeller were to fail, there would be no tendency for the wing to stall.

In this case, the local velocity seen by the airfoil section is simply the sum of the freestream and propeller induced velocity (i.e., $V_{ep} = V_\infty + V_p$). The percentage increase in the lift per unit span is equivalent to the percentage increase in the dynamic pressure. This relationship as well as an equivalent relationship in terms of the incoming velocity in the propeller slipstream and the freestream velocity are given in Eq. 15.

$$\frac{\Delta L'}{L'_\infty} = \frac{\Delta q}{q_\infty} = \frac{V_p}{V_\infty}\left(\frac{V_p}{V_\infty} + 2\right) \tag{15}$$

(Note that in other cases, we have developed expressions ignoring propeller thrust. Here, because the thrust is in the direction of the freestream velocity, Eq. 15 holds regardless of the thrust level.)

4. Propeller Normal Axis Inclined Downward Below the Freestream Velocity

For the case shown in Figure 7(d) in which $-i_p > \alpha_g$, we expect both the circulation strength and the local angle of attack of the airfoil to increase compared to the case with only the freestream velocity (i.e., $\Gamma_{\text{new}} > \Gamma_\infty$ and $\alpha_{ep} > \alpha_g$). The increased angle of attack has several ramifications that must be considered including:

1. The lift per unit span is tilted forward (in the "negative drag" direction), which implies that not all the force produced by the airfoil section is usable for lift, but some will help produce thrust.
2. In case of propeller loss, the airfoil angle of attack will suddenly decrease. Although it is advantageous that the wing section will not stall, there will still be a noticeable decrease in lift.
3. Care must be taken so that α_{ep} does not exceed the local stall angle, which may be difficult because this local effective angle of attack will vary with power setting. Additionally, if any portion of the wing is unblown, these sections will likely be operating considerably below their maximum lift point (because $\alpha_g < \alpha_{ep} \leq \alpha_{\text{stall}}$) unless there is a large geometric twist in the wing.

Eq. 9, which was given above in Section III.A.1 and is repeated below for convenience, is valid for this case, but here $\kappa > 1$.

$$\frac{\Delta L'}{L'_\infty} = \kappa \frac{V_{ep}}{V_\infty} - 1$$

Similarly, Eq. 10 and Eq. 11 are valid for this case as well; the only difference here is that $i_p < 0$.

As in Section III.A.1, the percentage lift increase can be compared to the change in dynamic pressure with Eq. 12, which is repeated below for convenience.

$$\frac{\Delta L'}{L'_\infty} = \frac{q_{\text{new}}\left(\sin\alpha_{ep}/\sin\alpha_g\right) - q_\infty}{q_\infty}$$

Here, $\sin\alpha_{ep}/\sin\alpha_g > 1$ because $\alpha_{ep} > \alpha_g$; therefore, the percentage increase in lift will be greater than that predicted when the thrust is aligned with the freestream velocity (Eq. 15). However, it is prudent to remember that this analysis does not capture stall and has ignored the fact that the thrust vector actually produces negative lift.

B. Extension to Three Dimensions

Although the expressions above for the percentage increase in lift per unit span were developed in two dimensions, they can be applied to provide a first-order estimate of the lift increase expected for a full wing. If the twist distribution of the wing behind a propeller is constant, then the percentage increase in the wing lift due to that single propeller can be estimated with Eq. 16

$$\frac{\Delta C_L}{C_{L_\infty}} = \left(\frac{\Delta L'}{L'_\infty}\right)\left(\frac{b_{\text{blown}}}{b}\right) \tag{16}$$

where $\Delta L'/L'_\infty$ can be determined from the equation above (either Eq. 11, 14, or 15) that is appropriate for the geometry under consideration, b is the wing span, and b_{blown} is the span of the wing immersed in the slipstream of the single propeller. This equation makes several assumptions in addition to those made above to determine $\Delta L'/L'_\infty$:

- Swirl is either negligible or the effects of swirl on one side of the propeller disk effectively cancel out the effects of swirl on the opposite side of the disk.
- The slipstream velocity is assumed to be constant behind the propeller. Because of this assumption, this model can very easily be paired with basic momentum theory,[5–7] which assumes a uniform velocity increase aft of a propeller disk. In reality, the velocity in the propeller slipstream will vary with radial station. If a radial variation of the velocity is known, either a single average velocity should be input into Eq. 16 or an integration of the two dimensional solutions for $\Delta L'/L'_\infty$ developed above should be performed.
- No section of the wing behind the propeller is at or near stall (i.e., all local wing sections are at angles of attack in the linear region of the lift curve)
- The propellers should not extend all the way to the wing tips. The flow at the airfoil sections near the tip cannot be approximated well by a two-dimensional airfoil and this method is incapable of capturing any interaction between the propeller vortex structure and wing tip vortex.

Eq. 16 can be generalized to account for wings with N propellers and/or sections of wing twist as shown in Eq. 17. In this equation, the percentage lift increase of the wing section i and the percentage of the span in the propeller slipstream of section i are combined with all other sections to give the net effect on the entire wing.

$$\frac{\Delta C_L}{C_{L_\infty}} = \sum_{i=1}^{N} \left(\frac{\Delta L'}{L'_\infty}\right)_i \left(\frac{b_{\text{blown}}}{b}\right)_i \tag{17}$$

C. Summary of the Two-Dimensional Model

For configurations in which the velocity over the wing is increased by the presence of a propeller slipstream, the orientation of the slipstream relative to the local airfoil sections can play a large role in the lift augmentation. Simple logic that estimates the lift augmentation to be directly proportional to the increase in dynamic pressure may lead to overly optimistic predictions of wing lift. Additionally, designers should not only consider the lift augmentation but also the safety implications of a particular configuration in case of a motor failure.

If the wing is operated so that the geometric angle of attack of many wing sections are at or near stall, the maximum lift benefit is expected when the propeller is inclined so that the thrust is directly aligned with the incoming freestream velocity vector (i.e., $i_p = -\alpha_g$) as shown in Figure 7(c). This installation is also advantageous because it should experience the least changes in wing lift in the case of a propeller failure.

If the wing is operated so that the geometric angle of attack of all wing sections are noticeably below stall, the maximum lift benefit may be experienced when the local propeller slipstream is angled above the incoming freestream velocity vector as shown in Figure 7(d) provided that the negative lift component from the thrust from the propellers is not too great and that the effective angle of attack remains below stall.

If the propeller thrust is very large, it may be most advantageous for the overall lift of the configuration to have a component of the thrust vector tilted in the lift direction (such as in Figure 7(a) or Figure 7(b)). However, these installations may be dangerous in the event of a motor failure due to the high likelihood of sections of the wing stalling that may lead to a spin.

IV. The Leading Edge Propeller as a High Lift Device

Traditionally propellers have been used primarily as propulsive devices; however, in designs similar to the concept shown in Figure 1, the function of the distributed propellers is to provide lift augmentation. The propellers can therefore be viewed as high lift devices. High lift devices such as flaps and slats are often characterized by the ways in which they modify the lift curve of an airfoil, e.g., the lift curve slope, zero-lift angle of attack, and stall lift coefficient. In this section we derive a relationship between the propeller slipstream velocity and installation angle with the apparent lift curve slope and zero-lift angle of attack.

For this analysis, we presume that the lift per unit span increases linearly with the angle of attack and that the lift per unit span is proportional to the incoming dynamic pressure to the wing section. If the wing section is fully immersed in a propeller slipstream as shown in Figure 3, the velocity vector diagram shown in Figure 4 will represent the local velocity at the airfoil. Therefore, the lift per unit span of the airfoil section can be expressed as Eq. 18, where the apparent velocity seen by the airfoil is $\boldsymbol{V_{ep}}$, a_0 is the nominal lift curve slope of the airfoil, and $\alpha_{L=0}$ is the nominal zero-lift angle of attack.

$$L' = \frac{1}{2}\rho V_{ep}^2 c a_0 \left[\alpha_{ep} - \alpha_{L=0}\right] \tag{18}$$

This expression can be written in terms of the local section lift coefficient, c_l, as shown in Eq. 19.

$$c_l = \frac{V_{ep}^2}{V_\infty^2} a_0 \left[\alpha_{ep} - \alpha_{L=0}\right] \tag{19}$$

When $\boldsymbol{V_{ep}} = \boldsymbol{V_\infty}$ and $\alpha_{ep} = \alpha_g$, Eq. 19 reduces to the typical form of a lift curve shown in Eq. 20.

$$c_l = a_0 \left[\alpha_g - \alpha_{L=0}\right] \tag{20}$$

For design purposes it is useful to obtain an expression of Eq. 19 that directly involves design variables for the propeller inclination angle and slipstream velocity. Such an expression can be obtained by substituting Eq. 5 and Eq. 3 into Eq. 19 for V_{ep} and α_{ep}, respectively. However, the complexity of the resulting equation limits insights.

A simpler expression can be obtained by presuming that the angles α_{ep}, α_g, i_p, and $\alpha_g + i_p$ are small. With these assumptions, α_{ep} can be represented by Eq. 4 and Eq. 5 reduces to $V_{ep} \approx V_\infty + V_p$. (Note that assuming $\alpha_g + i_p$ is small holds exactly for the case shown in Section III.A.3 in which the propeller slipstream is aligned with the freestream.) Under these assumptions, Eq. 19 reduces to Eq. 21

$$c_l \approx \left(1 + \frac{V_p}{V_\infty}\right) a_0 \left\{\alpha_g - \left[\alpha_{L=0}\left(1 + \frac{V_p}{V_\infty}\right) + \frac{V_p}{V_\infty} i_p\right]\right\} = \left(a_0\right)_{\text{apparent}} \left[\alpha_g - \left(\alpha_{L=0}\right)_{\text{apparent}}\right] \tag{21}$$

where the apparent lift curve slope and zero-lift angle of attack of the local airfoil section are defined in Eq. 22 and Eq. 23, respectively.

$$\left(a_0\right)_{\text{apparent}} = a_0 \left(1 + \frac{V_p}{V_\infty}\right) \tag{22}$$

$$\left(\alpha_{L=0}\right)_{\text{apparent}} = \alpha_{L=0}\left(1 + \frac{V_p}{V_\infty}\right) + \frac{V_p}{V_\infty} i_p \tag{23}$$

It is clear from Eq. 21 that the propeller slipstream velocity impacts both the apparent zero-lift angle of attack and the lift curve slope while the propeller inclination angle impacts only the former.

The variation of the lift curve of an airfoil for various values of the propeller slipstream velocity and inclination angle is illustrated in Figure 8. Figure 8(a) shows lift curves for a single airfoil at specific conditions, Figure 8(b) presents the increase in the lift curve slope, and Figures 8(c) and 8(d) show how the zero-lift angle of attack is modified for two nominal zero-lift angle of attack values.

Each of the lift curves shown in Figure 8(a) corresponds to an unblown airfoil with a nominal lift curve slope of 2π rad^{-1} and a zero-lift angle of attack of $-2°$. The lift curve for the base airfoil is shown with a thick solid black line. The other four lift curves are those predicted by Eq. 21 for slipstream velocities of $V_p = V_\infty$ and $V_p = 2V_\infty$ and slipstream inclination angles of $i_p = -5$ and $i_p = 0$. The net effect of the propeller blowing over the airfoil is to shift the lift curves up and to the left.

To observe how changes in the slipstream velocity affect the lift curve slope, we define a lift curve slope multiplier, K_{a_0}, as the ratio of the apparent lift curve slope to the nominal lift curve slope as shown in Eq. 24.

$$K_{a_0} = \frac{\left(a_0\right)_{\text{apparent}}}{a_0} = \left(1 + \frac{V_p}{V_\infty}\right) \tag{24}$$

The variation of the lift curve sloper multiplier with the slipstream velocity is shown in Figure 8(b). When the slipstream velocity is zero, the lift curve slope multiplier is unity, and K_{a_0} increases linearly with the

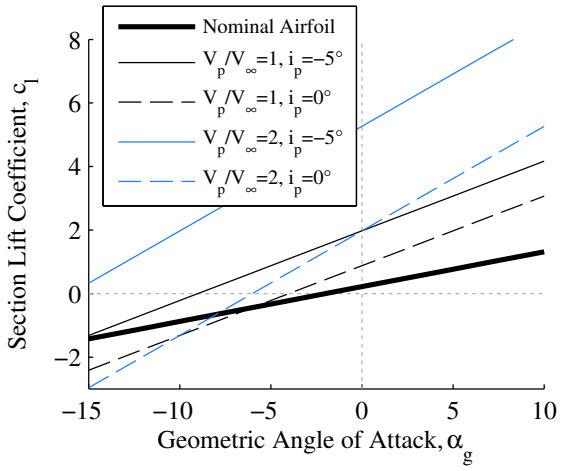

(a) Comparison of lift curves with different slipstream velocities and inclination angles for a baseline airfoil

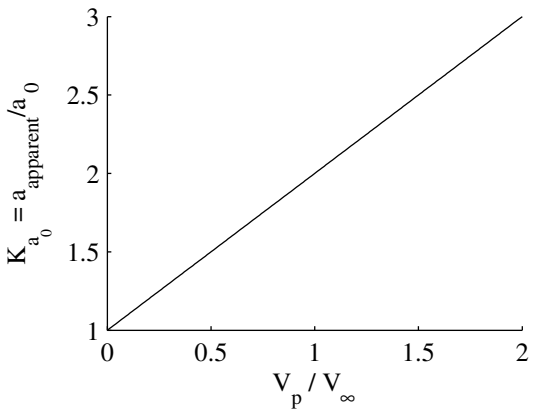

(b) Variation of the lift curve slope multiplier, K_{a_0}, with propeller slipstream velocity

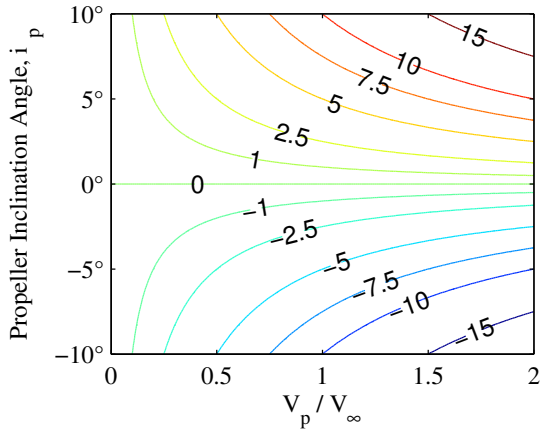

(c) Apparent zero-lift angle of attack as a function of propeller slipstream velocity and slipstream inclination angle for an airfoil with a nominal zero-lift angle of attack of 0°

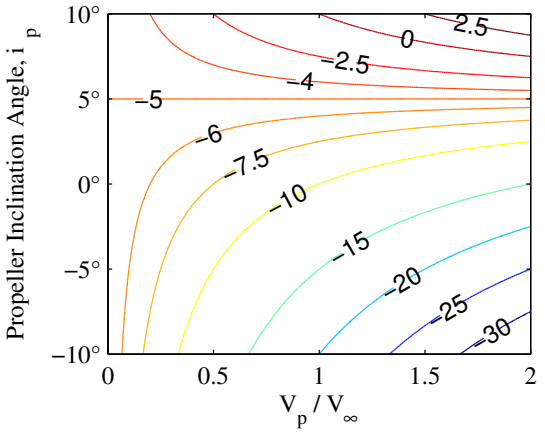

(d) Apparent zero-lift angle of attack as a function of propeller slipstream velocity and slipstream inclination angle for an airfoil with a nominal zero-lift angle of attack of −5°

Figure 8. Effect of propeller slipstream and slipstream inclination angle on the lift curve of an airfoil assuming a very large propeller slipstream height

slipstream velocity. This indicates that higher slipstream velocities will generate increased lift as would be expected.

The apparent zero-lift angle of attack varies with both the propeller slipstream velocity and inclination angle. Figures 8(c) and 8(d) show the variation of the apparent zero-lift angle of attack for airfoils with nominal zero-lift angles of attack of 0° and −5°, respectively. It is clear from these figures and Eq. 23 that the apparent zero-lift angle of attack is equivalent to the nominal zero-lift angle of attack for all slipstream velocities if the inclination angle is the negative of the nominal zero-lift angle of attack of the airfoil (i.e., if $i_p = -\alpha_{L=0}$). For inclination angles less than this value (i.e., $i_p < -\alpha_{L=0}$), the apparent zero-lift angle of attack is reduced compared to the nominal value (i.e., $(\alpha_{L=0})_{\text{apparent}} < \alpha_{L=0}$); similarly, if $i_p > -\alpha_{L=0}$, then $(\alpha_{L=0})_{\text{apparent}} > \alpha_{L=0}$.

V. Accounting for Propeller Slipstream Height

The above analysis has assumed that the airfoil section is completely immersed in a very wide slipstream flow. However, for designs such as that shown in Figure 1, the diameter of the propeller will likely not be large compared to the wing chord. Additionally, the contraction of the slipstream aft of the propeller will

further reduce the effective diameter of the slipstream relative to the diameter of the propeller. In general, it is of interest to be able to study configurations in which the diameter of the propeller is smaller than the wing chord. In these cases, the assumptions made in the simple models presented above will not directly hold and must be modified.

The flow around an airfoil in a propeller slipstream can be viewed as a special case of an airfoil in the vicinity of a boundary between multiple non-uniform streams. For cases where the propeller slipstream is aligned with the freestream velocity (i.e., where $i_p = -\alpha_g$), the problem reduces to an airfoil in non-uniform parallel streams. Such flows have been analyzed in the past.[9–12] The resulting geometry for such a flow is shown in Figure 9. In this figure, the airfoil is placed in a "jet" of finite height with velocity $V_j > V_\infty$. If the increased velocity in the jet is due to a propeller then $V_j = V_{ep} = V_\infty + V_p$ following the notation above. The height of the slipstream is denoted as $2h$ and the chord length of the airfoil is c.

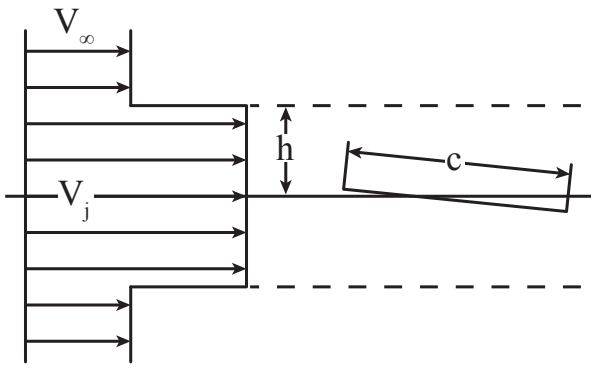

Figure 9. A flat plate airfoil placed in a slipstream of finite height

We now consider a flat plate in the slipstream of a propeller as shown in Figure 9. If the notation from the previous sections is maintained, then the geometry in the figure implies that $i_p = 0$, $\alpha_{ep} = \alpha_g$, and $V_j = V_{ep} = V_\infty + V_p$. The theory developed above in Section IV predicts the lift coefficient as Eq. 19, which can be written as Eq. 25 for the flat plate shown in Figure 9 that has $\alpha_{L=0} = 0$ and $a_0 = 2\pi$ rad^{-1}.

$$c_l = \frac{V_j^2}{V_\infty^2} (2\pi) \alpha_g \tag{25}$$

To compare the effects of different slipstream velocities on the lift of the flat plate, a lift multiplier, K_L, is defined as the ratio of the lift generated by a flat plate in a slipstream, c_l, and the lift produced by the flat plate in the absence of the slipstream, $(c_l)_\infty$. For the flat plate, which has a lift curve slope of 2π rad^{-1}, a zero-lift angle of attack of 0°, and a geometric angle of attack α_g, the lift multiplier can be expressed in several forms as shown in Eq. 26.

$$K_L = \frac{c_l}{(c_l)_\infty} = \frac{c_l}{2\pi\alpha_g} = \frac{V_j^2}{V_\infty^2} \tag{26}$$

For the case where $V_j = 2V_\infty$, the lift is predicted by the prior theory to increase by a factor of four (i.e., $K_L = 4$); similarly, if $V_j = 1.5V_\infty$, then $K_L = 2.25$.

In reality, these lift multiplier values of 4 and 2.25 are overly optimistic. Ting et al.[11] showed that for a finite slipstream height, the lift produced by an airfoil is less than if the airfoil were located in a single stream with velocity V_j. The effect of slipstream height on the flat plate lift is shown in Figure 10 for two values of V_j: $1.5V_\infty$ and $2V_\infty$.[11] As shown in the figure, the lift multiplier values predicted by the theory developed in Section IV of the present paper (i.e., Eq. 26) hold only in the limit as the height of the slipstream increases toward infinity. For geometries in which the height of the slipstream is on the order of twice the chord length or less (i.e., $h/c < 1$), we observe considerably smaller increases in lift as compared to the prior theory. In the limit as the slipstream height becomes infinitely small, the lift becomes equivalent to a flat plate in a freestream velocity of V_∞, and consequently $K_L = 1$.

To account for the effects of finite slipstream height, the theory presented in Sections III and IV is modified by applying a multiplicative factor, β, to the propeller slipstream velocity, V_p. This factor is

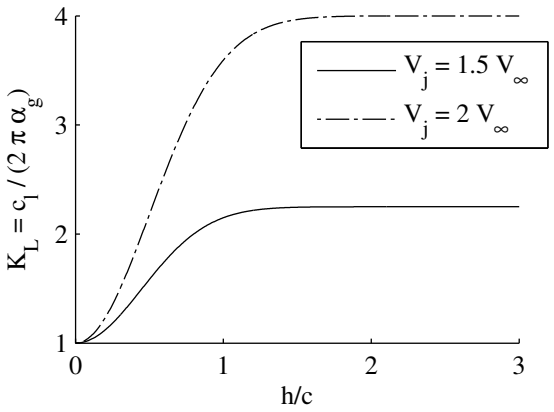

Figure 10. Effect of slipstream height on the lift produced by a flat plate [reproduced from[11]]

bounded between 0 and 1 with $\beta = 0$ corresponding to $h/c = 0$ and $\beta = 1$ strictly holding only in the limit as h/c approaches infinity. However, as can be observed from Figure 10, β reaches a value of effectively 1 at $h/c \approx 1.5$ because K_L approaches the values predicted for infinite slipstream heights there. In general, β is a nonlinear, sigmoid-like function of h/c.

Each of the equations in Section III predicting the lift increase $\Delta L'/L'_\infty$ (i.e., Eqs. 9 through 15) should be modified to include the β parameter. The inclusion of this parameter will reduce the lift increase predicted in all circumstances. For the sake of brevity, only the most general of these equations, Eq. 11, is presented here in Eq. 27 to illustrate how this modification is performed.

$$\frac{\Delta L'}{L'_\infty} = \left(1 - \frac{\beta V_p \sin i_p}{V_\infty \sin \alpha_g}\right) \frac{\sqrt{V_\infty^2 + 2V_\infty \beta V_p \cos(\alpha_g + i_p) + (\beta V_p)^2}}{V_\infty} - 1 \tag{27}$$

At different locations behind a propeller, the value of β will vary from a maximum to zero as the two-dimensional height of the propeller decreases from the diameter at the center to zero at the tip. In order to apply Eqs. 16 and 17 that extend Eq. 27 to three dimensions, a single "average" β value should be selected based on an average value for the slipstream height, $\bar{h}$. For a propeller of radius r, $\bar{h}$ can be selected as $r\pi/4$ such that the mass flow rate through the $2\bar{h}$ x $2r$ rectangle is equivalent to the mass flow rate through the circle with radius r.

The equations in Section IV should also be modified with the parameter β to account for finite slipstream height. With this modification, Eq. 21 can be rewritten as Eq. 28.

$$c_l \approx \left(1 + \frac{\beta V_p}{V_\infty}\right) a_0 \left[\alpha_g - \left(\alpha_{L=0}\left(1 + \frac{\beta V_p}{V_\infty}\right) + \frac{\beta V_p}{V_\infty} i_p\right)\right] \tag{28}$$

The apparent lift curve slope and the apparent zero-lift angle of attack of the local airfoil section are therefore modified to Eq. 29 and Eq. 30, respectively.

$$(a_0)_{\text{apparent}} = a_0 \left(1 + \frac{\beta V_p}{V_\infty}\right) \tag{29}$$

$$(\alpha_{L=0})_{\text{apparent}} = \alpha_{L=0}\left(1 + \frac{\beta V_p}{V_\infty}\right) + \frac{\beta V_p}{V_\infty} i_p \tag{30}$$

Figure 11 shows five lift curves for a baseline airfoil with $a_0 = 2\pi$ rad^{-1} and $\alpha_{L=0} = -2°$ with two slipstream velocities and two slipstream heights. As seen before in Figure 8(a), the lift curves in the presence of the propeller slipstream are shifted up and to the left. However, for finite slipstream heights (i.e., $\beta < 1$), the shifting of the lift curve is reduced compared to the value predicted with an infinite slipstream height. This can be seen in Figure 11 by comparing either of the two sets of curves with equivalent slipstream velocity

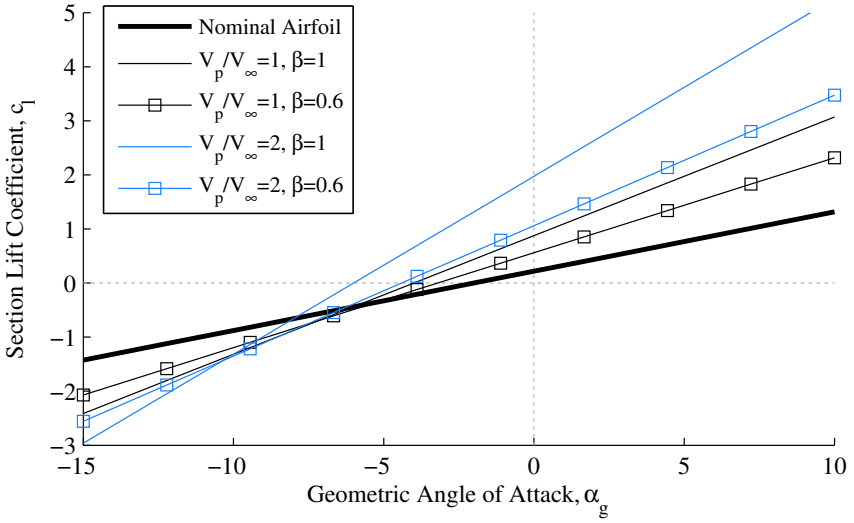

Figure 11. Comparison of lift curves for a baseline airfoil in propeller slipstreams of various velocities and heights

ratios but different β values. The slipstream height affects both the apparent zero-lift angle of attack as well as the lift curve slope.

To isolate the effects of a finite slipstream height on the lift curve slope, a new lift curve slope multiplier defined in Eq. 31 indicates how changes in both the propeller slipstream velocity and height affect the lift curve slope.

$$K_{a_0} = \frac{(a_0)_{\text{apparent}}}{a_0} = \left(1 + \frac{\beta V_p}{V_\infty}\right) \tag{31}$$

Figure 12 shows contours of the lift curve slope multiplier for values of β ranging from 0 to 1 (i.e., slipstream heights ranging from zero to infinite) and for slipstream velocities varying from $V_j = V_\infty$ (i.e., the case with no slipstream) to $V_j = 3V_\infty$.

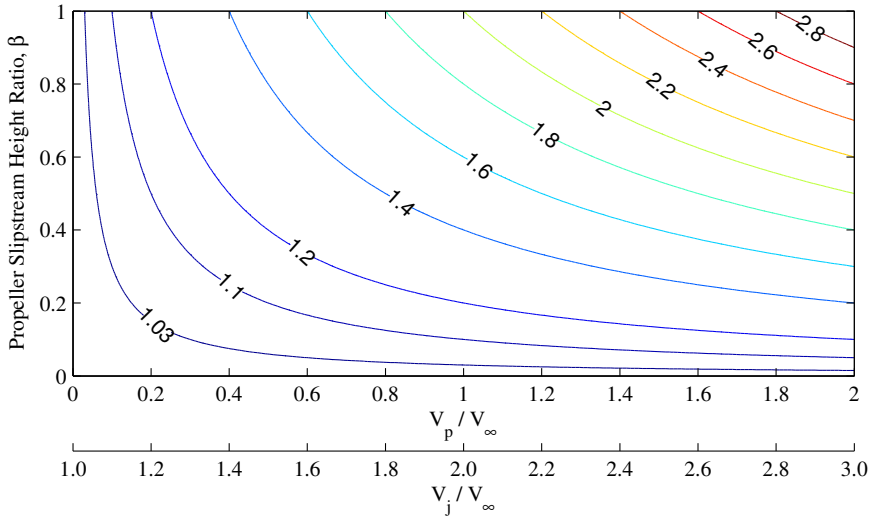

Figure 12. Contours of the lift curve slope multiplier, K_{a_0}, for various values of the propeller slipstream velocity and slipstream height

For low values of β (i.e., small slipstream heights), the lift curve slope multiplier shows relatively little variation with propeller slipstream velocity. This indicates that if the slipstream height is too small, the slipstream velocity is relatively unimportant. This behavior implies a practical lower limit to the leading edge propeller diameters to provide appreciable lift augmentation. For high slipstream velocities, the lift curve slope multiplier is highly dependent on the slipstream height. If propellers are designed with high induced velocities, the effects of the slipstream height will potentially play a significant role in the lift augmentation achievable for those configurations.

The effects of the slipstream height and velocity on the apparent zero-lift angle of attack are shown in Figure 13 for two airfoils with $i_p = 0$ and nominal zero-lift angles of attack of $-10°$ and $-2°$. These contours follow the same pattern as those in Figure 12 for the lift curve slope multiplier. At low slipstream velocities the effect of the slipstream height is small and at low slipstream heights the effect of the slipstream velocity is small. At high slipstream velocities there is a strong coupling between the apparent zero-lift angle of attack and the slipstream height.

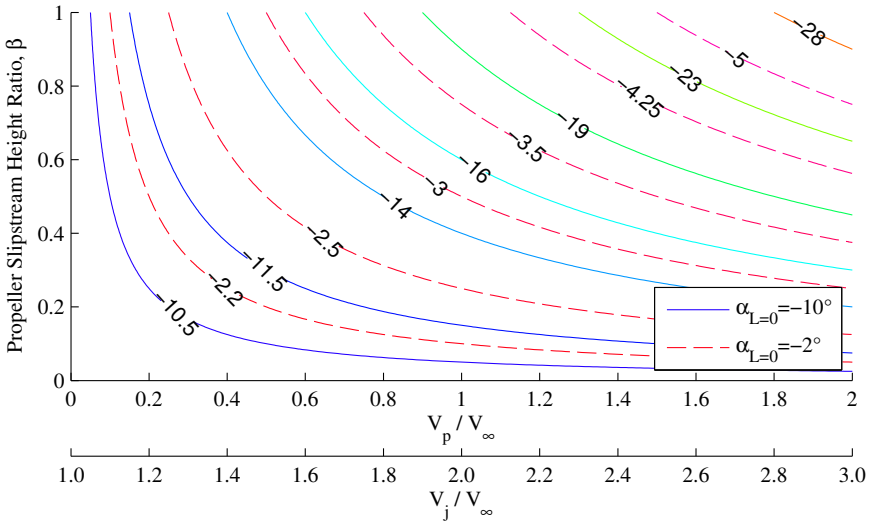

Figure 13. Contours of the apparent zero-lift angle of attack in degrees for various values of the propeller slipstream velocity and slipstream height with $i_p = 0$ and nominal airfoil zero-lift angles of attack of $-10°$ (shown in solid lines) and $-2°$ (shown in dashed lines)

VI. Conclusions

Simplified aerodynamics models to predict the effects of upstream propellers on wing lift have been presented. These models predict only the effects of leading edge propellers on wing lift while neglecting any influence of the wing on the propeller flow. The initial model presented assumes that the propeller slipstream diameter is very large compared with the local chord length, which is likely a poor assumption for configurations of interest. Therefore, the results from the this method are non-conservative and should be interpreted as an upper bound.

The initial model indicates that the angle at which the upstream propellers are installed may have significant impacts on the wing lift augmentation; therefore, propeller installation angles must be considered in early design to obtain accurate sizing estimates. It is likely most advantageous both from lift augmentation and safety viewpoints to install the propellers such that the propeller slipstream velocity closely aligns with the freestream angle of attack during conditions where the leading edge propellers operate. Other factors such as propeller thrust contribution to lift and nacelle drag in cruise must also be considered and may affect the choice of installation angle. Nonetheless, this simple model provides a mechanism to rapidly assess how various installations may affect wing lift augmentation.

In viewing the upstream propellers as high lift devices, it is instructive to derive the effects of the slipstream on the lift curve slope and zero-lift angle of attack of the blown airfoil sections. The velocity,

height, and angle of the slipstream will all affect the lift as described in Section V. All of these effects must be considered to produce accurate estimates from analysis of configurations with distributed leading edge propellers. Increases in slipstream velocity and height both shift the lift curve up and to the left when compared with the baseline airfoil. Under small angle assumptions, the slipstream inclination angle, i_p, affects only the apparent zero-lift angle of attack and, in general, decreasing i_p shifts the lift curve to the left (reduces the apparent zero-lift angle of attack).

Designers of aircraft with leading edge propellers for lift augmentation will face inherent tradeoffs in the ideal diameter of the propellers. Simple momentum theory indicates that very small diameters are likely advantageous for increasing the slipstream velocity, which is beneficial for lift augmentation. However, if the propeller diameter is too small, then the lift augmentation from the increased slipstream velocity may be drastically reduced from that predicted assuming the slipstream height were large. It is anticipated that ideal high lift propeller diameters will be on the order of the wing chord length, but detailed higher-order studies should be performed for each configuration to determine this ideal propeller size.

Acknowledgments

This work has been supported by the NASA Aeronautics Scholarship Program through grant number NNX14AE59H. The authors would like to thank Dr. Nicholas Borer and Mark Moore from the NASA Langley Research Center for their support and guidance in this effort.

References

[1]Moore, M. D. and Fredericks, B., "Misconceptions of Electric Aircraft and their Emerging Aviation Markets," *52nd Aerospace Sciences Meeting*, 2014, AIAA 2014-0535.

[2]Stoll, A. M., Bevirt, J., Moore, M. D., Fredericks, W. J., and Borer, N. K., "Drag Reduction Through Distributed Electric Propulsion," *14th AIAA Aviation Technology, Integration, and Operations Conference*, Atlanta, GA, 16–20 June 2014, AIAA 2014-2851.

[3]Borer, N. K., Moore, M. D., and Turnbull, A., "Tradespace Exploration of Distributed Propulsors for Advanced On-Demand Mobility Concepts," *14th AIAA Aviation Technology, Integration, and Operations Conference*, Atlanta, GA, 16–20 June 2014, AIAA 2014-2850.

[4]Patterson, M. D., Daskilewicz, M. J., and German, B. J., "Conceptual Design of Electric Aircraft with Distributed Propellers: Multidisciplinary Analysis Needs and Aerodynamic Modeling Development," *52nd Aerospace Sciences Meeting*, National Harbor, MD, 13–17 January 2014, AIAA 2014-0534.

[5]Rankine, W. J. M., "On the Mechanical Principles of the Action of Propellers," *Transactions of the Institute of Naval Architects*, Vol. 6, 1865, pp. 13–39.

[6]Froude, R. E., "On the Part Played in Propulsion by Differences of Fluid Pressure," *Transactions of the Institute of Naval Architects*, Vol. 30, 1889, pp. 390–405.

[7]McCormick, Jr., B. W., *Aerodynamics of V/STOL Flight*, Dover, Mineola, New York, 1999.

[8]Anderson, Jr., J. D., *Fundamentals of Aerodynamics*, McGraw Hill, 4th ed., 2005.

[9]Ting, L. and Liu, C., "Thin Airfoil in Nonuniform Parallel Streams," *Journal of Aircraft*, Vol. 6, No. 2, 1969, pp. 173–175.

[10]Chow, F., Krause, E., Liu, C. H., and Mao, J., "Numerical Investigations of an Airfoil in a Nonuniform Stream," *Journal of Aircraft*, Vol. 7, No. 6, 1970, pp. 531–537.

[11]Ting, L., Liu, C. H., and Kleinstein, G., "Interference of Wing and Multipropellers," *AIAA Journal*, Vol. 10, No. 7, 1972, pp. 906–914.

[12]Prabhu, R. K. and Tiwari, S. N., "Linearized Potential Solution for an Airfoil in Nonuniform Parallel Streams," NASA-CR-173047, National Aeronautics and Space Administration, August 1983.